LWT - Food Science and Technology 242 (2026) 119124

Contents lists available at ScienceDirect

LWT

journal homepage: www.elsevier.com/locate/lwt

Impact of pH shifting on structural and emulsifying characteristics of whey protein isolate amyloid fibrils

Caiyun Cheng [a], Qian Xu [a], Yang Li [b], Eric Haubruge [c], Ning Liao [a], Guangsu Zhu [a], Kunlun Liu [a,*]

[a] College of Food Science and Engineering, Henan University of Technology, Zhengzhou, 450001, China
[b] Mengniu Institute of Nutrition Science, Global R&D Innovation Center, Inner Mongolia Mengniu Dairy (Group) Co., Ltd., Beijing, 101107, China
[c] Gastronomic Sciences Lab, University of Liege - Gembloux Agro-Bio Tech, 2 Passage des Déportés, Gembloux, 5030, Belgium

ARTICLE INFO

Keywords:
Whey protein isolate
Protein amyloid fibrils
Pickering emulsion
Structural features
Emulsifying characteristics

ABSTRACT

Whey protein isolate amyloid fibrils (WPIFs) were prepared via acidic thermal treatment at pH 2.0, 85 °C for10 h. The aim was to investigate the influence of different pH values (2.0–8.0) on the structural features of WPIFs and emulsifying properties of WPIFs-stabilized Pickering emulsions. Thioflavin T (ThT) fluorescence confirmed WPIFs formation at pH 2.0. Transmission electron microscopy (TEM) and atomic force microscopy (AFM) revealed that WPIFs maintained long fibrils at pH 2.0–3.0, whereas short fibrils were observed at pH 7.0–8.0. At pH 4.0–6.0, WPIFs underwent aggregation which resulted in increased particle size and decreased zeta potential, with the most distinct aggregates forming at pH 5.0. The structure of WPIFs affected by pH changes determined the emulsification of WPIFs Pickering emulsions. Specifically, WPIFs at pH 5.0 exhibited relatively low emulsifying activity index (EAI) of 14.84 ± 0.37 m^2/g and high emulsifying stability index (ESI) of 93.25 ± 1.54%. WPIFs Pickering emulsion at pH 5.0 showed increased droplet sizes and enhanced viscoelasticity. The results indicated that the emulsifying properties of WPIFs Pickering emulsions were dependent on the structural features of WPIFs. These findings provide valuable insights into the pH-dependent structural regulation of WPIFs and highlight the application prospects of amyloid fibril-stabilized Pickering emulsions.

1. Introduction

Protein amyloid fibrils can be formed by heating protein solutions under controlled conditions (Mohammadian & Madadlou, 2018). Initially, amyloid fibrils were regarded as pathological aggregates closely associated with debilitating neurodegenerative diseases such as Alzheimer's, Parkinson's, and type II diabetes mellitus (Khan & Khan, 2022). Subsequent studies have indicated that the formation of amyloid fibrils is a common characteristic of proteins (Cao & Mezzenga, 2019). Both in vitro and in vivo studies have demonstrated that food-derived protein amyloid fibrils are safe nutritional components for human health (Jansens et al., 2019). Their unique morphological structures and functional characteristics make them ideal candidates for the development of novel functional food ingredients (Zhang et al., 2024). As an innovative approach for protein modification, protein amyloid fibrils have attracted increasing scientific interest. Notably, protein amyloid fibrils exhibit distinctive structural characteristics, such as high stiffness, high interfacial modulus, high aspect ratio, and high hydrogen bond network, endowing proteins with functional properties, including thickening, gelation, foaming, emulsification, film formation, and adsorption (Meng et al., 2022). Specifically, Zhao et al. (2025) reported that soy protein amyloid fibrils, as promising emulsifiers and gelling agents, can be efficiently adsorbed at the oil-water interface and embedded in the gel network, thus holding broad application prospects in emulsion-based and gel-based foods. Meanwhile, Qi et al. (2024) and Ouyang et al. (2024) demonstrated that rice protein amyloid fibrils and whey protein amyloid fibrils, acting as potential foaming and thickening agents, are capable of enhancing the foaming capacity of angel food cake and optimizing the textural structure of fermented yogurt, respectively. Furthermore, Zheng et al. (2024) found that the incorporation of whey protein amyloid fibrils into edible film-forming matrices improved the tensile strength and barrier properties of the resulting packaging materials, while also effectively inhibiting the browning of fresh-cut apples and reducing moisture loss of cheddar cheese.

In the pursuit of sustainable and innovative development within the food industry, the high-value utilization of by-products has become a

* Corresponding author.
E-mail address: knlnliu@126.com (K. Liu).

https://doi.org/10.1016/j.lwt.2026.119124
Received 14 August 2025; Received in revised form 30 January 2026; Accepted 2 February 2026
Available online 3 February 2026

strategic imperative. Whey protein isolate (WPI), the primary by-product of casein production, contains all essential amino acids, which exhibits excellent nutritional value and diverse functional characteristics (Zeng et al., 2024; Zhu, 2024). WPIFs are typically formed under extreme acidic conditions (pH 2.0). This acidic environment significantly promotes the formation of whey protein isolate amyloid fibrils (WPIFs), which can pose challenges for practical food processing applications. Specifically, the acidic environment exceeds the acceptable range for food processing, as the pH range of most foods typically falls from 4.0 to 7.0 to ensure safety, taste, and overall quality. Deviating from this acceptable range can lead to undesirable alterations in texture, flavor, and nutritional value (Ouyang et al., 2024; Xu, Zhang, et al., 2024). It is therefore necessary to consider how pH shifting away from the acidic environment influences the structural features of WPIFs, thereby facilitating their broader application in food processing. In addition, pH shifting not only affects the structural features of WPIFs, but also further influences their emulsifying properties. Therefore, the objective of this study was to investigate the influence of pH values (2.0–8.0) on the structural features of WPIFs and the emulsifying properties of WPIFs-stabilized Pickering emulsion.

Different denaturation conditions, including strong acid environments, salt types and concentrations, heat treatments, enzymatic hydrolysis, and organic solvents, can all induce protein fibrillation while exerting a notable impact on the fibrillation process and the structural characteristics of the resulting amyloid fibrils. Among these approaches, long-term acidic thermal treatment is a simple and efficient strategy for preparing protein amyloid fibrils. In this study, WPIFs were prepared by heating WPI solution (3%, w/v) at 85 °C for 10 h under acidic conditions (pH 2.0). The pH value of the WPIFs solution was adjusted to the range of 2.0–8.0, and the structural features of WPIFs and the emulsifying properties of WPIFs-stabilized Pickering emulsions at pH 2.0–8.0 were systematically investigated.

2. Materials and methods

2.1. Materials

WPI (protein concentration ≥97%) was supplied by Fonterra Company (Auckland, New Zealand). Thioflavin T (ThT) and 1-anilino-8-naphthalenesulfonate (ANS) were purchased from Aladdin Biochemical Technology Co., Ltd. (Shanghai, China). The Bradford kit was obtained from Shanghai Solarbio Bio-Technology Co., Ltd. (Shanghai, China). Soybean oil was purchased from Yihai Kerry Arawana Holdings Co., Ltd. (Shanghai, China). All chemicals and reagents used in this study were of analytical grade.

2.2. WPIFs preparation

WPIFs were prepared via the acidic thermal method with minor modifications (Xu et al., 2025). Firstly, WPI was dissolved in deionized water to obtain a 3% (w/v) WPI solution, magnetically stirred for 30 min, and then fully hydrated at 4 °C overnight. Subsequently, the solution was adjusted to pH 2.0 with 2 M HCl. The WPI solution was placed in a magnetic stirrer and incubated at 85 °C for 10 h to obtain the WPIFs solutions. After incubation, the heated WPIFs solutions was immediately cooled to 25 °C in an ice bath. The WPIFs solution was then adjusted to the target pH values (2.0–8.0) with 1 M NaOH. Finally, the concentration of the WPIFs solutions was measured using the Bradford assay and adjusted to 1 mg/mL with deionized water pre-adjusted to the corresponding pH values. The WPIFs samples were stored at 4 °C or freeze-dried for further studies.

2.3. ThT fluorescence measurement

The ThT fluorescence intensity of WPIFs solution at pH 2.0–8.0 was determined using a fluorescence spectrophotometer (F-7000, Hitachi, Tokyo, Japan) (Xu et al., 2025). 7.9 mg of ThT was dissolved in 10 mL of phosphate buffer solution (10 mM phosphate, 150 mM NaCl, pH 7.4) to prepare ThT stock solution. ThT stock solution was diluted 50 times with phosphate buffer solution to obtain ThT working solution. WPIFs solutions were diluted to 0.1 mg/mL using deionized water pre-adjusted to the corresponding pH values. 40 μL of diluted WPIFs solutions was mixed with 4 mL of ThT working solution. The excitation wavelength was set at 460 nm and the emission wavelength was collected over the range of 480–600 nm. Slit widths of excitation and emission were both 5 nm, and the scan speed was 1200 nm/min. ThT working solution (without WPIFs) was used as the background and then subtracted to obtain the corrected differential fluorescence spectrum.

2.4. Intrinsic fluorescence measurement

The intrinsic fluorescence of WPIFs solutions at pH 2.0–8.0 was determined using a fluorescence spectrophotometer (F-7000, Hitachi, Tokyo, Japan) (H. Zhao, Xu, Yuan, Qi, & Li, 2024). The excitation wavelength was set at 280 nm and the emission wavelength was collected over the range of 300–500 nm. Slit widths of excitation and emission were both 5 nm, and the scan speed was 1200 nm/min.

2.5. Size distribution and zeta potential measurement

The size distribution and zeta potential of WPIFs solutions at pH 2.0–8.0 were determined using a Zetasizer (BT-90, Bettersize, China) (Ouyang et al., 2023). WPIFs solutions were diluted to 0.1 mg/mL using deionized water pre-adjusted to the corresponding pH values. The refractive indices of the protein and water were 1.450 and 1.333, respectively. The equilibration time was 120 s and each measurement was performed three times at 25 °C.

2.6. Turbidity measurement

The turbidity of WPIFs solutions at pH 2.0–8.0 was determined using a UV spectrophotometer (TU-1900, Puxi, China) (Jiang, Pan, et al., 2022). WPIFs solutions were diluted to 0.2 mg/mL using deionized water pre-adjusted to the corresponding pH values, and the transmittance (T) was measured at 600 nm. The turbidity of WPIFs solutions was calculated as (100-T)% with deionized water used as the blank control.

2.7. Surface hydrophobicity (H_0) measurement

The surface hydrophobicity of WPIFs solutions at pH 2.0–8.0 was determined by the external ANS fluorescence probe method with some modifications (Pang et al., 2020). In brief, WPIFs solutions were diluted to 0.1 mg/mL using distilled water pre-adjusted to the corresponding pH values. 4 mL of WPIFs solutions was mixed with 40 μL of ANS solution (8.0 mM, pH 7.0). The mixture was incubated in the dark for 20 min at room temperature, after which the fluorescence intensity was recorded using a fluorescence spectrophotometer (F-7100, Hitachi Corp., Japan). The excitation wavelength was set at 390 nm, and emission wavelength was collected over the range of 400–600 nm. Slit widths of excitation and emission were both 5 nm, and the scan speed was 1200 nm/min.

2.8. Fourier transform infrared spectroscopy (FTIR) measurement

The secondary structure of WPIFs at pH 2.0–8.0 was determined using a Fourier transform infrared (FTIR) spectrometer (Nicolet 6700, Thermo, Germany), following the method described by Ji et al. (2021). Spectral scanning was performed over the range of 500–4000 cm^{-1}, with a resolution of 4 cm^{-1} and 32 scans. The secondary structure content was quantified within the amide I band (1600-1700 cm^{-1}) via peak deconvolution. OMNIC 8.0 software was used for spectral preprocessing, and PeakFit software (v4.12) was used for peak-fitting

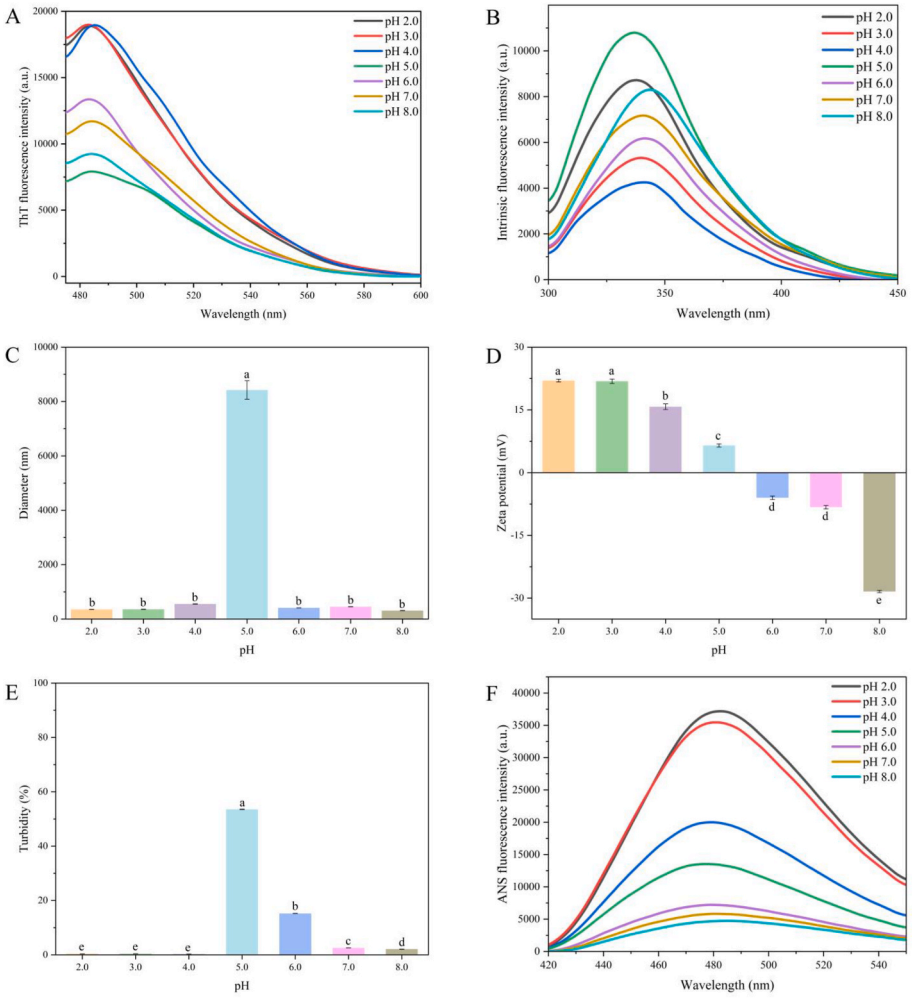

Fig. 1. ThT fluorescence (A), intrinsic fluorescence (B), average size (C), zeta potential (D), turbidity (E), and ANS fluorescence (F) of WPIFs solutions as a function of pH 2.0–8.0. Different lowercase letters on the results indicate a significant difference ($P < 0.05$).

analysis.

2.9. Transmission electron microscope (TEM) measurement

The morphological structure of WPIFs at pH 2.0–8.0 conditions was observed using a TEM instrument (HT-7700, Hitachi, Japan). 10 μL of WPIFs solutions was deposited onto carbon-coated copper grids and then left to stand in a dry environment for 30 min. Afterward, TEM images were collected at an accelerating voltage of 100 kV.

2.10. Atomic force microscopy (AFM) measurement

The detailed morphological structure of WPIFs at pH 2.0–8.0 conditions was observed using an AFM apparatus (MFP-3D Infinity, Oxford, USA)0.10 μL of WPIFs solutions was deposited onto freshly cleaved mica substrates (1.0×1.0 cm^2) and then air-dried at room temperature. AFM data processing was performed using Asylum Research 16.23.224 and Fiber App software to analyze the morphology, height distribution, and periodicity of WPIFs at pH 2.0–8.0.

2.11. WPIFs-stabilized Pickering emulsions preparation

WPIFs-stabilized Pickering emulsions at pH 2.0–8.0 were prepared using the high speed shear emulsification method as previously reported (Cheng et al., 2024). WPIFs solutions (3%, w/v) were mixed with the soybean oil phase (60%, v/v) for emulsification. The mixed systems were homogenized at 25000 r/min for 3 min to obtain WPIFs Pickering emulsions. Pickering emulsions at pH 2.0–8.0 were stored in cylindrical glass bottles for further analysis.

2.12. Emulsifying properties measurement

The emulsifying activity and emulsifying stability of WPIFs Pickering emulsions at pH 2.0–8.0 were measured using a UV spectrophotometer (TU-1900, Puxi, China). Fresh emulsions (10 μL) were diluted 400 times with the SDS solution (1.0 mg/mL) and mixed thoroughly. The absorbance of the diluted emulsions was measured at 500 nm with SDS solution used as a reference. Eq. (1) and Eq. (2) were used to calculate the emulsifying activity index (EAI) and the emulsifying stability index (ESI).

$$\mathrm{EAI}\ (\mathrm{m}^2/\mathrm{g}) = \frac{2 \times 2.303 \times A_0 \times N}{\mathrm{C} \times \varphi \times 10^4} \quad (1)$$

$$\mathrm{ESI}\ (\%) = \frac{A_{30}}{A_0} \times 100\% \quad (2)$$

Where EAI is emulsifying activity index (m^2/g), ESI is emulsifying stability index (%), A_0 and A_{20} are the absorbance of the WPIFs Pickering emulsions at 0 min and 30 min, N is the dilution factor (100), C is the protein concentration (mg/mL), and φ represents the oil volume fraction (0.6).

2.13. Microstructure observation

The morphological structure of WPIFs Pickering emulsions at pH 2.0–8.0 was observed using an optical microscope (DM1000, Leica, Germany). Fresh emulsions (2 μL) were directly dropped onto the microscope slide and then observed at 200 × magnification. The droplet sizes of Pickering emulsions at pH 2.0–8.0 were calculated using Nano Measurer 1.2 software.

2.14. Rheology measurement

The rheological properties of WPIFs Pickering emulsions at pH 2.0–8.0 were determined using a rheometer (MARS60, HAAKE, Germany) (Cheng et al., 2023). A CC50 parallel plate geometry measuring system (50 mm diameter, 1.0 mm gap) was used for amplitude sweep, frequency sweep, and flow sweep measurement. Amplitude sweep was conducted in the strain range of 0.001–100% with a frequency of 1.0 rad/s at 25 °C to obtain the linear viscoelastic region (LVR). Frequency sweep was performed over an angular frequency range of 1–100 rad/s at 25 °C within the linear viscoelastic range (0.01%) to record storage modulus (G′) and loss modulus (G″). Flow sweep was measured with a shear rate of 0.1–100 s^{-1} at 25 °C.

2.15. Statistical analysis

Each measurement was carried out in duplicate, and experimental data were expressed as the mean ± standard deviation (SD) of the three samples in each group. Data results were analyzed using SPSS (v26.0, SPSS Inc.) and Origin 2021 (Origin Lab Inc.). Differences between-groups were analyzed using one-way analysis of variance (ANOVA) and Duncan's multiple range test. Values of $P < 0.05$ were considered statistically significant.

3. Results and discussion

3.1. Characteristics of WPIFs at pH 2.0–8.0

3.1.1. ThT fluorescence analysis

Thioflavin (ThT), a cationic benzothiazole fluorophore, can specifically bind to the cross β-sheet structure of protein amyloid fibrils through hydrophobic interactions. ThT fluorescence assay is widely recognized as the gold standard for detecting the presence of cross β-sheet structure, identifying the formation of protein amyloid fibrils (Chang et al., 2017). ThT fluorescence intensity of WPIFs solutions as a function of pH 2.0–8.0 is shown in Fig. 1(A). WPIFs exhibited the highest ThT fluorescence intensity at pH 2.0–4.0, indicating a high abundance of cross β-sheet structures within WPIFs under this pH range. ThT molecules specifically bind to the cross β-sheet domains of WPIFs, maintaining the excited state and thereby resulting in a high quantum yield of fluorescence, which is manifested as a significant increase in fluorescence intensity (Farrokhi et al., 2019). As illustrated in Fig. 1(A), ThT fluorescence intensity at pH 6.0–8.0 was significantly lower than that at pH 2.0–4.0, and the lowest ThT fluorescence intensity of WPIFs was recorded at pH 5.0. These findings suggested that the abundance of detectable amyloid fibrils decreased with increasing pH. The decrease in ThT fluorescence intensity was attributed to either the partial destruction of amyloid fibrils or the reduction of available ThT binding sites in amyloid fibrils in agreement with Lin et al. (2025). Chen et al. (2022) also reported that the maximum ThT fluorescence intensity of WPIFs at pH 7.0 was lower than that at pH 2.0, which was attributed to the disruption of fibril structures or the loss of β-sheets.

3.1.2. Intrinsic fluorescence analysis

Intrinsic fluorescence spectra measured at an excitation wavelength of 280 nm are commonly used to reflect conformational changes in the tertiary structure and reveal alterations in polar and nonpolar environments (J. Xu, Tang, Wang, Xie, & Xu, 2024). Intrinsic fluorescence intensity of WPIFs solutions as a function of pH 2.0–8.0 is shown in Fig. 1(B). The changes in the intrinsic fluorescence intensity and the maximum emission wavelength of WPIFs solutions depended on the exposure degree of tryptophan residues, which act as the main chromogenic group. As presented in Fig. 1(B), the maximum emission wavelength of WPIFs redshifted from 335 nm to 345 nm at pH 8.0, indicating an increase in the microenvironmental polarity of tryptophan residues. This phenomenon occurred due to the fact that the alkaline environment significantly promoted the dissolution of WPIFs, thereby causing WPIFs to be exposed to the surrounding water. In addition, the decreasing trend in fluorescence intensity demonstrated the presence of a steric hindrance between WPIFs and fluorescence signal (Ouyang et al., 2023). The maximum fluorescence intensity of WPIFs at pH 5.0 was higher than that at pH 2.0, which suggests that the exposure of hydrophobic groups within the WPIFs was more pronounced at pH 5.0. This phenomenon also confirmed that the amyloid fibril structures of WPIFs underwent significant changes at pH 5.0.

3.1.3. Size and zeta potential analysis

The average size of WPIFs solutions measured by dynamic light scattering can reflect the aggregation behavior of the WPIFs solutions under different pH environments (Koo, Chung, Ogren, et al., 2018). The average size of WPIFs solutions as a function of pH 2.0–8.0 is shown in Fig. 1(C). Across the pH range of 2.0–8.0, the average size of WPIFs was the largest at pH 5.0. The isoelectric point of WPIFs was known to be pH 5.2 (Lin et al., 2023). Since pH 5.0 is close to the isoelectric point of WPIFs, and the reduction in electrostatic was insufficient to maintain the stability of amyloid fibrils at pH 5.0, leading to the aggregation of WPIFs. The formation of WPIFs aggregates at pH 5.0 enhanced the scattering intensity, thus increasing the average size of WPIFs. As depicted in Fig. 1(C), when the pH was far from 5.0, strong electrostatic repulsion existed between amyloid fibrils, causing the aggregates to dissipate and the average size to drop sharply to 309.62 ± 4.25 nm. It was worth noting that WPIFs were in fibril structures, and dynamic light scattering is only used to provide evidence of the aggregation behavior of WPIFs induced by pH shifting (Meng et al., 2024).

Zeta potential reflects the dispersion stability and surface charge density of WPIFs solutions under different pH environments. Generally, the absolute value of zeta potential greater than 20 mV indicates that solutions have good dispersion and stability. The Zeta potential of WPIFs solutions as a function of pH 2.0–8.0 is shown in Fig. 1(D). It has been reported that the isoelectric points of WPI and WPIFs are pH 4.4 and pH 5.2 respectively (Lin et al., 2023). The shift of the isoelectric point was attributed to the ability of long-term acid heat treatment to induce conformational changes in WPI. This process resulted in the exposure of different charged groups or the chemical degradation of certain charged groups, thereby rendering the protein more anionic (Cui et al., 2022). As displayed in Fig. 1(D), Zeta potential decreased from 21.99 ± 0.33 mV to 6.51 ± 0.38 mV as the pH increased from 2.0 to 5.0, and increased from 6.51 ± 0.38 mV to about 28.43 ± 0.26 mV as the pH increased from 5.0 to 8.0. The WPIFs solutions carried positive or negative charges, which were determined by the pH environment of WPIFs solutions (Chen et al., 2020). pH range of 2.0–5.0 is lower than the isoelectric point of WPIFs. The dissociation of the carboxyl groups of amyloid fibrils was inhibited, and the corresponding amino groups were over protonated, resulting in WPIFs carrying a positive charge at pH 2.0–5.0. pH 5.0 is close to the isoelectric point of WPIFs. The protonation of the amino groups and the deprotonation of the carboxyl groups reach equilibrium, leading to the charge of WPIFs approaching zero at pH 5.0. pH range of 6.0–8.0 is higher than the isoelectric point of WPIFs. The dissociation of amino groups of amyloid fibrils is inhibited, and the corresponding carboxyl groups are over deprotonated, resulting in WPIFs carrying a negative charge at pH 6.0–8.0. In contrast, the zeta potential of WPIFs was the lowest at pH 5.0, implying that the solution environment close to the isoelectric point reduced the electrostatic

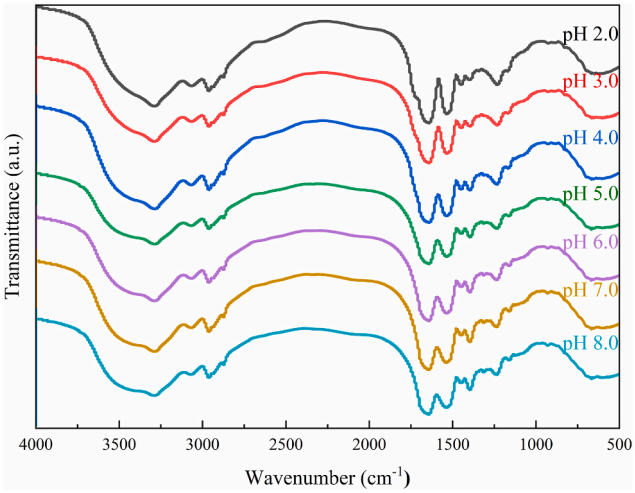

Fig. 2. FTIR spectra of WPIFs at pH 2.0–8.0.

repulsion between WPIFs molecules. Low charge density of WPIFs weakened the interparticle repulsion between WPIFs molecules, resulting in aggregation and an increase in particle size.

3.1.4. Turbidity analysis

Light transmission measurement can provide insights into the aggregation behavior of WPIFs under different pH environments. The turbidity of WPIFs solutions as a function of pH 2.0–8.0 is depicted in Fig. 1(E). WPIFs solutions remained clear and transparent with low turbidity at pH 2.0–4.0, and no significant differences were observed among these pH values. The turbidity of WPIFs solution at pH 5.0 exhibited maximum turbidity (53.54 ± 0.09%). The bottom of the WPIFs solution became turbid at pH 5.0 due to the formation of a micellar layer, thereby reducing the light transmittance. This increase in turbidity can be attributed to the fact that the environmental pH was close to the isoelectric point of WPIFs, reducing electrostatic repulsion and causing WPIFs to flocculate and precipitation to form large aggregates (Koo, Chung, Ogren, et al., 2018). These findings were consistent with the result of size and zeta potential. With a further increase in pH from 5.0 to 8.0, the turbidity gradually decreased and the solutions became nearly transparent, indicating the disappearance of WPIFs aggregates. In summary, the variation in electrostatic repulsion in WPIFs solution significantly affected the aggregation morphology of WPIFs molecules.

3.1.5. Surface hydrophobicity (H_0) analysis

ANS fluorescence probe assay is a commonly used approach for evaluating the surface hydrophobicity of proteins. The fluorescence intensity of ANS binding to hydrophobic groups is positively correlated with the H_0 of proteins. Changes in surface hydrophobicity reflect the exposure of the hydrophobic region of WPIFs under different pH environments, which influences their molecular conformation and functional properties. The H_0 of WPIFs solutions as a function of pH 2.0–8.0 is shown in Fig. 1(F). WPIFs exhibited higher surface hydrophobicity at pH 2.0 and 3.0, indicating that WPIFs molecules exposed more hydrophobic groups at pH 2.0 and 3.0, promoting the binding of ANS to the hydrophobic groups. As shown in Fig. 1(F), the order of the H_0 of WPIFs solutions was as follows: pH 2.0 > pH 3.0 > pH 4.0 > pH 5.0 > pH 6.0 > pH 7.0 > pH 8.0. The fluorescence intensity of ANS bound to WPIFs decreased as the pH increased from 2.0 to 8.0, indicating the pH environments affected the exposure of hydrophobic groups in WPIFs solution, thereby altering its surface hydrophobicity at different pH levels. It is worth noting that the surface hydrophobicity of WPIFs solutions under different pH conditions might not be entirely accurate (Cui et al., 2022). To the left of the isoelectric point of WPIFs, there is a strong attraction between the anion ANS and the positively charged WPIFs, which leads to an increase in the binding of ANS and thus overestimates the surface hydrophobicity. To the right of the isoelectric point of WPIFs, there is a strong repulsion between the anion ANS and the negatively charged WPIFs, which leads to a reduction in the binding of ANS and thus undervalues the surface hydrophobicity.

3.1.6. Fourier transform infrared spectroscopy (FTIR) analysis

FTIR, a powerful vibrational spectroscopy technique, provides invaluable information on hydrogen bonding and polypeptide backbone conformation of WPIFs in different pH environments (Y. Zheng, Gao, Chang, Sun, & Fang, 2023). The FTIR spectra of WPIFs solutions as a function of pH 2.0–8.0 are shown in Fig. 2. The typical characteristic peak regions in the FTIR spectra of WPIFs are the amide I band (1700-1600 cm^{-1}, ~1650 cm^{-1}, C=O stretching vibration), the amide II band (1600-1500 cm^{-1}, ~1550 cm^{-1}, C-N stretching vibration and N-H bending vibration), and the amide III band (1400-1200 cm^{-1}, ~1330 cm^{-1}, C-N stretching vibration and N-H bending vibration) (Meng et al., 2024). The amide II band and amide III band of WPIFs under different pH conditions were similar and showed no significant changes. As shown in Fig. 2, the amide I band of WPIFs spectra at pH 2.0–8.0 exhibited different peak intensities. It indicated that pH-shifting might change the interaction between WPIFs molecules. To further explore the secondary structure changes of WPIFs under different pH conditions, the self-deconvolution and peak fitting analysis of the amide I spectrum (1600–1700 cm^{-1}) within the FTIR spectrum were carried out using PeakFit software, and five secondary structures were identified. Usually, parallel β-sheet, antiparallel β-sheet, β-turn, α-helix, and random coil are identified as peaks with wavenumber range was 1630 cm^{-1}, 1617 and 1684 cm^{-1}, 1672 cm^{-1}, 1658 cm^{-1}, 1645 cm^{-1}, respectively (Farrokhi et al., 2020). Correspondingly, the secondary structure content of WPIFs at pH 2.0–8.0 was evaluated by calculating the peak area, as detailed in Table 1. The secondary structure of WPIFs is composed of regular structure and irregular structure, the regular structure is characterized by α-helix and β-sheet, and the irregular structure is characterized by β-turn and random coil. As the pH of the WPIFs solutions increased from 2.0 to 8.0, the content of parallel β-sheet and antiparallel β-sheet showed a trend of first decreasing and then increasing. This was attributed to the change in pH value altering the secondary structure of WPIFs, resulting in the aggregation and rearrangement of WPIFs. When nearing the

Table 1
Secondary structure content WPIFs at pH 2.0–8.0.

Sample	Antiparallel β-sheet (%)	Parallel β-sheet (%)	AP/P parallel β-sheet (%)	Random coil (%)	α-Helix (%)	β-Turn (%)
pH 2.0	20.74 ± 0.20^{a}	21.19 ± 0.20^{ab}	0.98 ± 0.02^{ab}	23.62 ± 0.10^{b}	19.78 ± 0.20^{c}	14.68 ± 0.30^{a}
pH 3.0	19.82 ± 0.30^{a}	21.45 ± 0.10^{a}	0.92 ± 0.01^{bc}	23.57 ± 0.10^{b}	20.25 ± 0.30^{bc}	14.92 ± 0.20^{a}
pH 4.0	19.85 ± 0.30^{a}	$20.33 \pm 0.20c^{d}$	0.98 ± 0.03^{ab}	23.63 ± 0.20^{b}	20.77 ± 0.20^{b}	15.42 ± 0.50^{a}
pH 5.0	16.74 ± 0.20^{c}	19.81 ± 0.30^{de}	0.85 ± 0.01^{d}	25.31 ± 0.10^{a}	22.02 ± 0.40^{a}	16.12 ± 0.10^{a}
pH 6.0	18.21 ± 0.30^{b}	20.68 ± 0.10^{bc}	0.88 ± 0.02^{cd}	24.27 ± 0.20^{b}	21.89 ± 0.20^{a}	14.95 ± 0.20^{a}
pH 7.0	20.29 ± 0.30^{a}	19.68 ± 0.10^{e}	1.03 ± 0.02^{a}	23.62 ± 0.20^{b}	19.78 ± 0.20^{c}	16.62 ± 0.20^{a}
pH 8.0	20.04 ± 0.50^{a}	20.40 ± 0.14^{cd}	0.98 ± 0.02^{ab}	24.07 ± 0.40^{b}	20.28 ± 0.30^{bc}	15.21 ± 1.34^{a}

Note: Different letters represent significant differences ($P < 0.05$). The AP/P β-sheet ratio was the ratio of antiparallel to parallel β-sheet content of proteins.

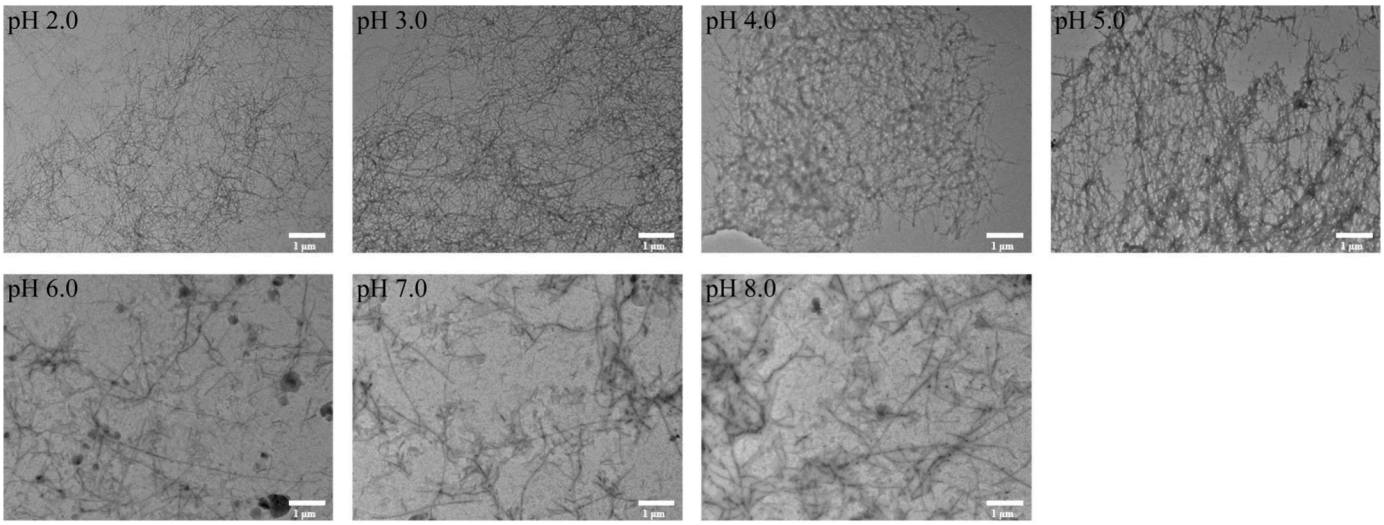

Fig. 3. TEM images of WPIFs at pH 2.0–8.0.

isoelectric point, WPIFs undergoes aggregation, while moving away from the isoelectric point results in depolymerization. In addition, the ratio of antiparallel β-sheet to parallel β-sheet can serve as an indicator of the structural polymorphism of WPIFs. Changes in this ratio in WPIFs solutions between pH 2.0 and 8.0 indicate pH-driven structural transformation of WPIFs.

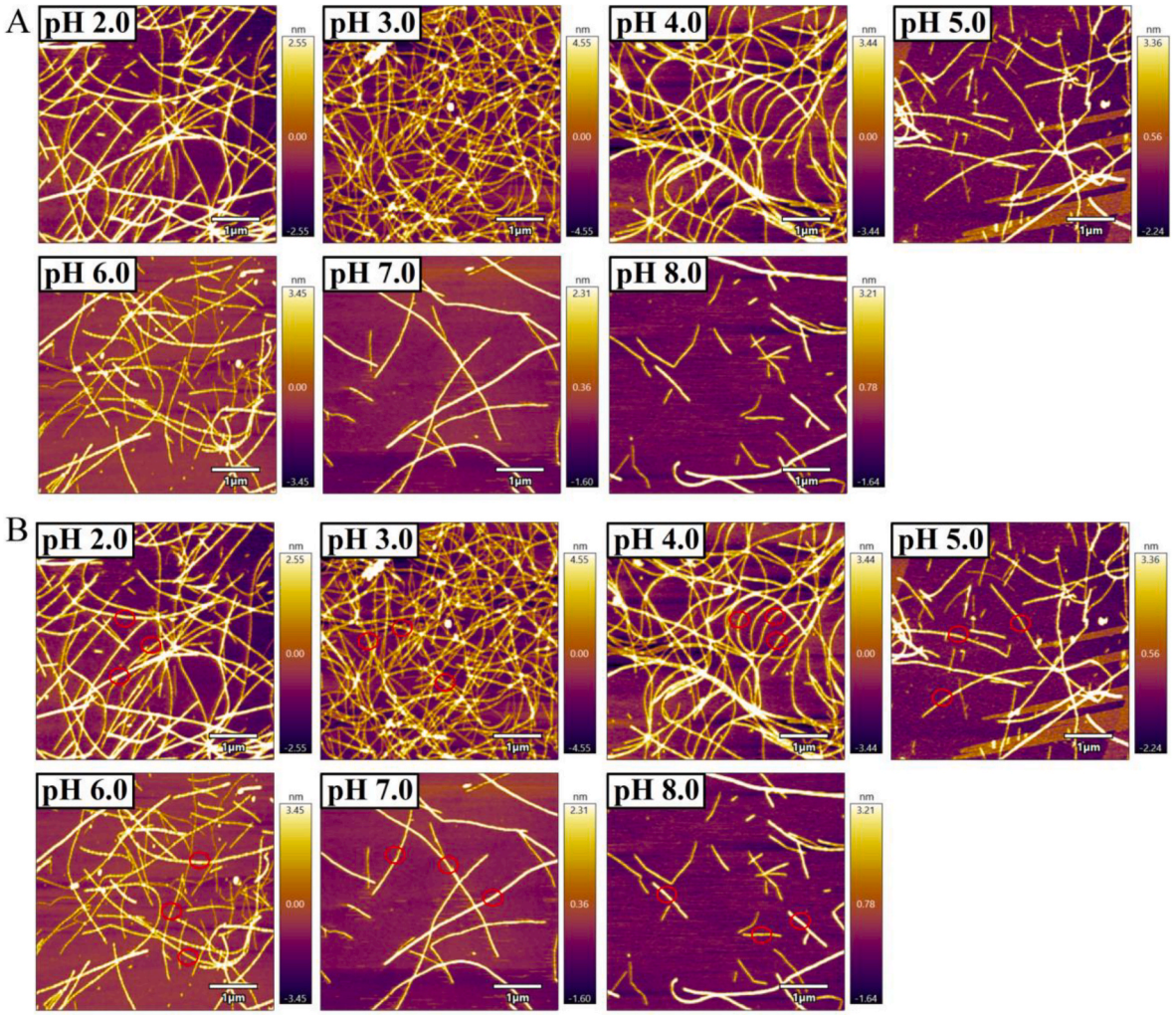

Fig. 4. Mesoscopic polymorphisms of WPIFs at pH 2.0–8.0. A: taken at 20 × 20 μm^2 (scale bar = 4 μm); B: taken at 5 × 5 μm^2 (scale bar = 1 μm). C: Height; D: Periodicity.

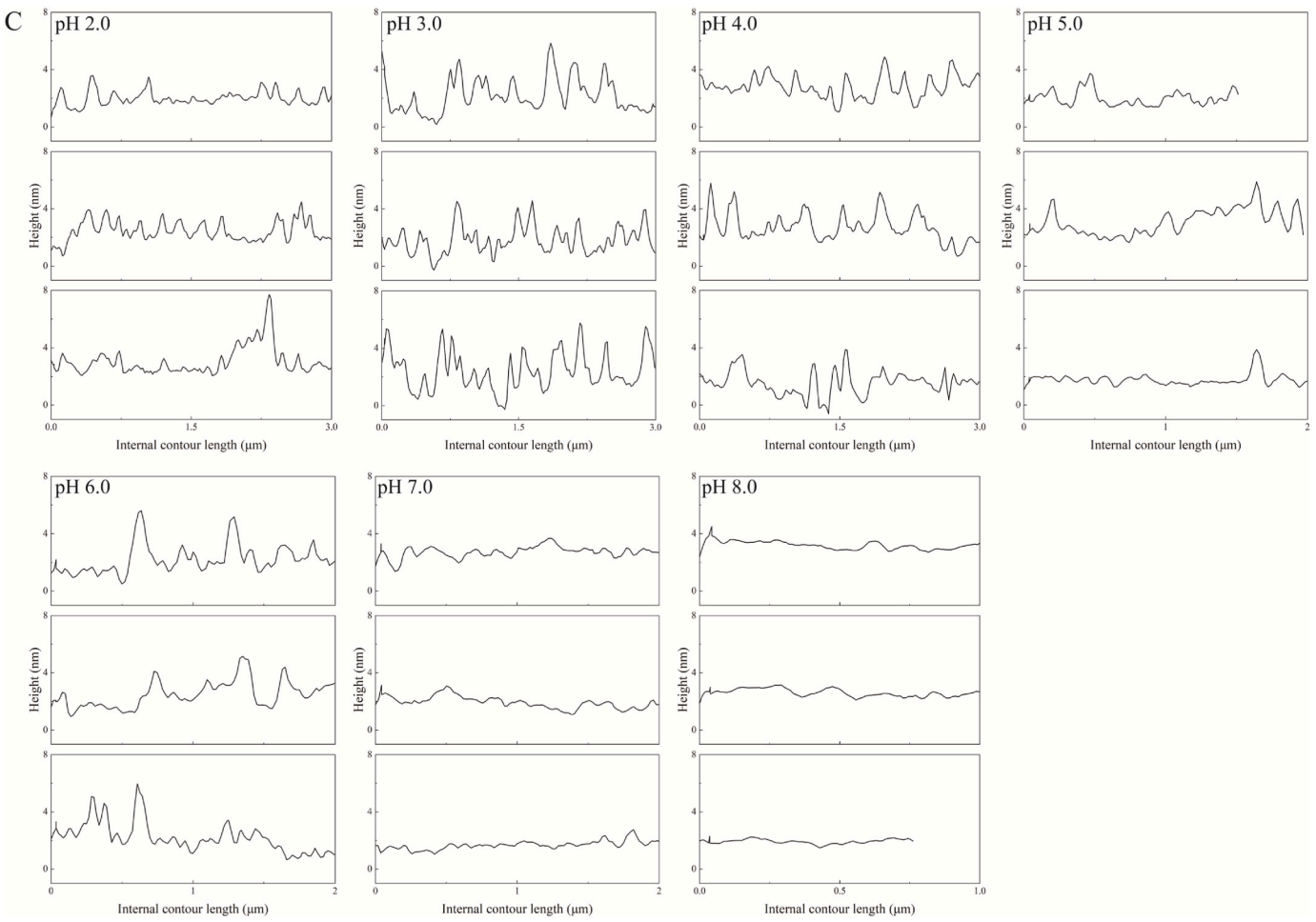

Fig. 4. (*continued*).

3.1.7. Transmission electron microscope (TEM) analysis

The morphology and microstructure of WPIFs as a function of pH 2.0–8.0 are depicted in Fig. 3. The diameter, length, and arrangement of WPIFs at pH 2.0–8.0 showed significant variations. Elongated and unbranched flexible amyloid fibrils with a length of several micrometers were observed in WPIFs at pH 2.0 and pH 3.0, exhibiting a uniform WPIFs network distribution. Slight entanglement could be observed between amyloid fibrils to form a loose network at pH 4.0. At pH 5.0, WPIFs began to aggregate or entangle to form large fibril aggregates. This is consistent with the changes in zeta potential, average particle size, and turbidity observed in previous experiments, which was attributed to the reduction of electrostatic repulsion between WPIFs at pH 5.0 near its isoelectric point, which made WPIFs molecules more closely bound together and strongly interact strongly on molecular surface, thereby forming more irregular and uneven aggregates. As the pH increased to 6.0–8.0, short amyloid fibril fragments were visible, whose length was significantly shorter than that of WPIFs at pH 2.0 and 3.0. This was attributed to the slightly weakening of WPIFs aggregations were at pH 7.0–8.0, with electrostatic repulsion existed between negatively charged WPIFs at pH 7.0–8.0. The fibril network was dissociated, leading to the dissociation of the fibril network and the formation of short fibrils and branched structures. Large fibril aggregates could be observed where the fibers overlapped, and entangled with each other, forming a dense cluster-like aggregate structures, producing a small amount of globular proteins. This is due to the fibril network to dissociate, resulting in separation, entanglement, integrity loss, or fragmentation (Jiang, Pan, et al., 2022). In conclusion, the impact of pH on the length of WPIFs is mainly attributed to electrostatic interactions. pH changes the charge density around WPIFs, affecting the interaction (attraction and repulsion) of WPIFs molecules to alter the morphological structure of amyloid fibrils.

3.1.8. Atomic force microscopy (AFM) analysis

AFM, a high-resolution technique for capturing nanoscale three-dimensional structures, has been extensively employed to investigate the morphological polymorphism and structural heterogeneity of protein amyloid fibrils. AFM images of WPIFs at the pH range of 2.0–8.0 are presented in Fig. 4(A), which confirmed that WPIFs possessed nanoscale diameter and a microscale length. These results clearly demonstrated that WPIFs maintained similar amyloid fibril structures at the pH range of 2.0–8.0, yet exhibited distinctly different contour lengths and persistence lengths. At pH 2.0 and 3.0, WPIFs formed interconnected, dense, and uniform fibril networks. At pH 4.0 and 5.0, WPIFs exhibited a tendency to entangle with one another, forming aggregated states with spiral winding. As the isoelectric point of WPIFs has been reported to be around 5.2, approaching this pH environment accelerated the entanglement between amyloid fibrils, thereby promoting the formation of fibril aggregates. At pH 6.0, 7.0, and 8.0, WPIFs presented mixed fibril fragments with heterogeneous lengths. The discrepancy could be attributed to the perturbation induced by the pH environment.

To further investigate the detailed features of WPIFs at the pH range of 2.0–8.0, we captured and magnified the corresponding AFM images as shown in Fig. 4(B). Representative amyloid fibrils were selected to analyze the length, height, and periodicity using Igor Pro 6.38 and Fiber App software. As illustrated in the magnified AFM images, WPIFs displayed long and flexible fibrils at pH 2.0–4.0, whereas short and rigid

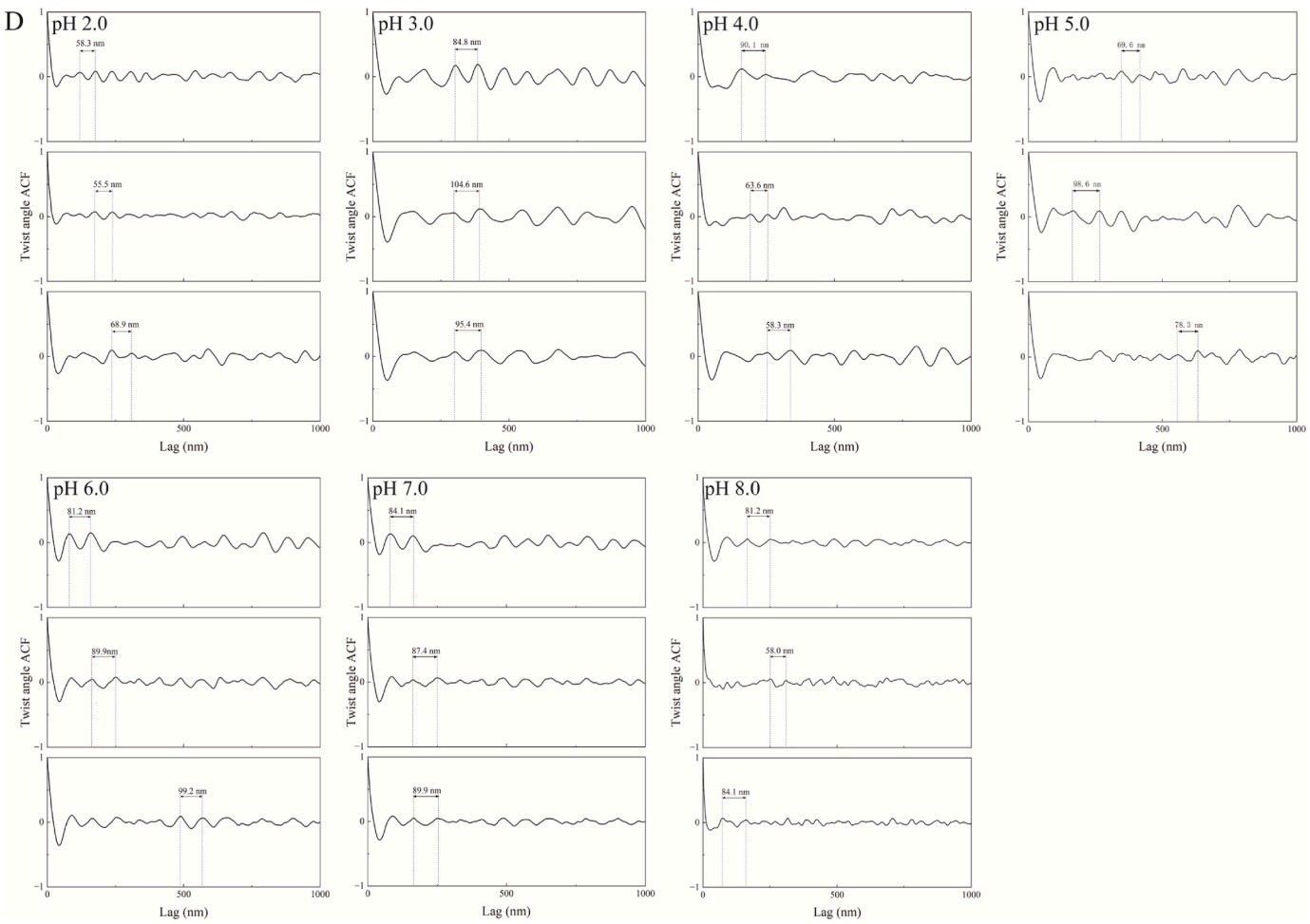

Fig. 4. (*continued*).

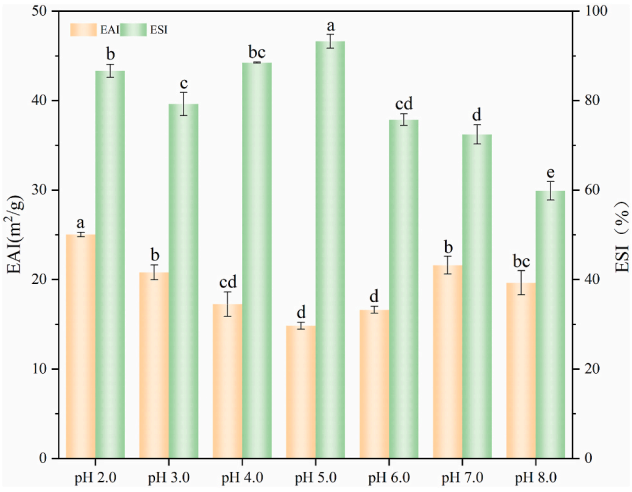

Fig. 5. Emulsifying activity and emulsifying stability of WPIFs-stabilized Pickering emulsions at pH 2.0–8.0.

fibrils were observed at pH 8.0. At pH 5.0–7.0, WPIFs exhibited a mixed morphology comprising both long fibrils and short fibrils. These results suggested that different pH environments have a significant impact on the length, height and periodicity of fibrils. Fig. 4(C) and (D) illustrated the serrated height distribution and periodic twist angle of WPIFs at pH 2.0–8.0, which are characteristic of twisted ribbon structures. As seen in the height profiles and the twist angle patterns, the serrated height distribution exhibited a decreasing trend with increasing pH, while the periodicity of twist angle showed an increasing trend with increasing pH, signifying that the fibril structure gradually loosened. This phenomenon could be attributed to the dissociation and breakage of the fibril structure induced by pH variations. At pH 2.0–4.0, the length profiles of WPIFs were calculated to exceed 4.0 μm and the height distribution was below 8.0 nm, indicating very high aspect ratio. At pH 5.0–8.0, the height of WPIFs was measured at around 4.0 nm and the periodicity ranged from 60 to 100 nm. Collectively, these analyses revealed that different pH environments have a significant impact on the length, height and periodicity of WPIFs, with fibrils shifting from long, flexible to short, rigid as the pH values increased.

3.2. Characteristics of WPIFs-stabilized Pickering emulsion at pH 2.0–8.0

3.2.1. Emulsifying properties analysis

The emulsifying properties of WPIFs were investigated by evaluating the EAI and ESI at pH 2.0–8.0. The EAI and ESI of WPIFs at pH 2.0–8.0 are shown in Fig. 5. WPIFs at pH 2.0 exhibited excellent EAI (25.03 ± 0.24 m^2/g) and ESI (86.65 ± 1.47 m^2/g). Liu, Liu, et al. (2024) have reported the potential of WPIFs as emulsifiers for stabilizing Pickering emulsions at pH 2.0. Interestingly, the emulsifying activity of WPIFs showed a trend of first decreasing and then increasing, while the emulsifying stability showed a trend of first increasing and then decreasing with increasing pH values. Among these pH values, pH 5.0 was a key turning point for the alteration of EAI (14.84 ± 0.37 m^2/g) and ESI (93.25 ± 1.54 %). This was speculated to be related to the fibril

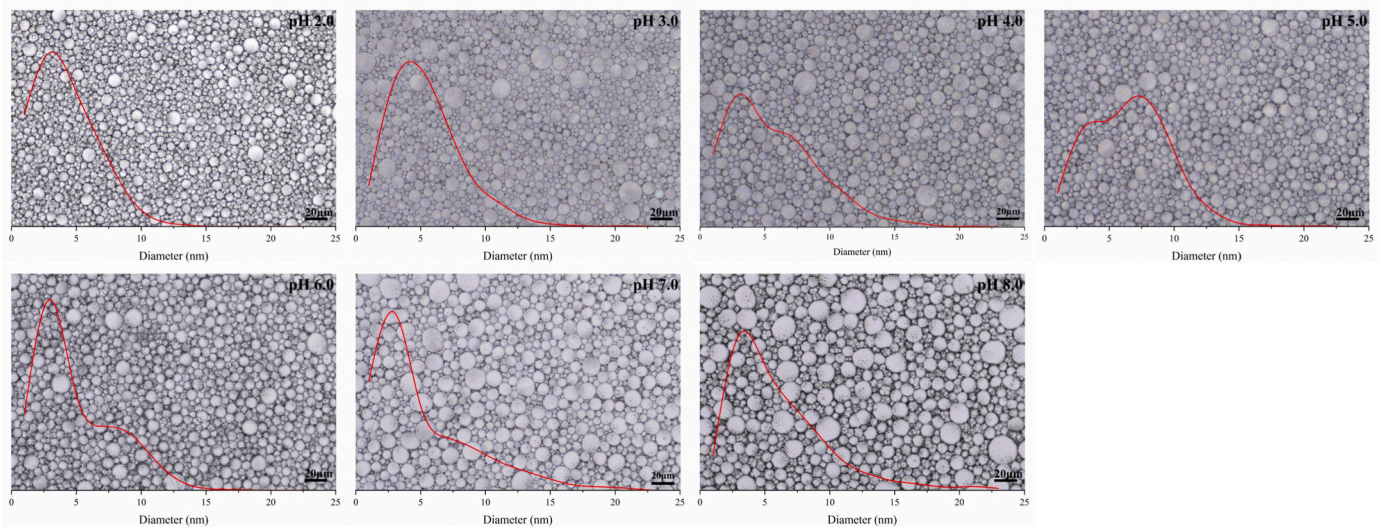

Fig. 6. Microscopy images and size distribution of WPIFs-stabilized Pickering emulsions at pH 2.0–8.0.

structures and droplet morphology. Ouyang et al. (2023) have reported WPIFs exhibited better emulsifying stability in near-neutral pH, especially at pH 5.5. This could be attributed to larger specific surface area of the emulsion droplets. Previous studies have also shown that WPIFs aggregated to become shorter and thicker at pH 4.0–6.0, and when used to stabilize Pickering emulsions, they exhibit a lower creaming index (Jiang, Pan, et al., 2022).

3.2.2. *Microstructure observation analysis*

The optical microscopy images and size distribution of WPIFs Pickering emulsions as a function of pH 2.0–8.0 are shown in Fig. 6. The possible stabilization mechanism of WPIFs-stabilized Pickering emulsion was that WPIFs adsorbed at the oil-water interface and formed an interfacial film to stabilize Pickering emulsion. This interface film can act as a spatial barrier to resist the flocculation and coalescence of emulsion droplets (G. Liu, Li, Qin, & Zhong, 2020). WPIFs Pickering emulsions exhibited dense morphology with closely arranged droplets. However, size distribution curves of WPIFs Pickering emulsions showed significant differences at pH 2.0–8.0. As illustrated in Fig. 6, the emulsion droplets varied significantly at pH 4.0–6.0, and the corresponding size distribution curves showed broad peaks or bimodal peaks. One possible explanation is that the morphology of the interfacial film of WPIFs-stabilized Pickering emulsions was altered at pH 4.0–6.0. WPIFs Pickering emulsions had narrow size distributions at pH 2.0 and 3.0, indicating that long fibrils stabilized Pickering emulsion with relatively smaller droplets. WPIFs Pickering emulsions had broader size distributions at pH 7.0 and 8.0, demonstrating that short fibrils stabilized Pickering emulsions with relatively larger droplets. It is worth noting that at pH 5.0, the WPIFs Pickering emulsion exhibited tighter droplet accumulation and broader size distributions, which was attributed to the clustering of WPIFs into fibril aggregates at this pH (Gao et al., 2017). This is consistent with the aggregates formation near the isoelectric point reported by Cui et al. (2022). Pickering emulsion stabilized by WPIFs aggregates had thicker interfacial layers, but it also caused the aggregation and uneven arrangement of emulsion droplets. This phenomenon can be attributed to the fact that the electrostatic repulsion of WPIFs weakens when the pH approaches the isoelectric point.

3.2.3. *Rheology analysis*

The rheological behavior of Pickering emulsion reflects the microscopic interactions between emulsion droplets and plays an important role in the stability of Pickering emulsion (Ju et al., 2024). To explore this further, amplitude sweep, frequency sweep, and flow behavior were conducted on WPIFs Pickering emulsion to thoroughly investigate their rheological properties at pH 2.0–8.0. Strain sweep measurements were performed over a strain range of 0.001–100% at a fixed frequency of 1.0 rad/s. Linear viscoelastic region (LVR) is defined as strain region where Storage modulus (G′) and loss modulus (G″) were almost independent of amplitude strain, characterized by constant G′ and G″ modulus even with increasing strain (Wang et al., 2023). G′ and G″ as a function of strain amplitude (0.001–100%) are displayed in Fig. 7(A). WPIFs Pickering emulsion are in LVR at a strain of 0.01%. Thus, a strain of 0.01% was selected for subsequent frequency sweep measurements. As illustrated in Fig. 7(A)–G′ and G″ of WPIFs Pickering were nearly independent of strain within the LVR. Moreover, G′ was always greater than G″, indicating that WPIFs Pickering emulsion exhibited elasticity-dominated rheological behavior at the low strain region, characteristic of a solid-like system. Once the strain exceeded the LVR, G′ showed a downward trend, while G″ first increased and then decreased, and G″ gradually became greater than G′. This suggested that WPIFs Pickering emulsion displayed viscosity-dominated rheological behavior at the high strain region, features of a liquid-like system. Pickering emulsion stabilized by WPIFs complexes showed the similar behavior (Lin et al., 2023).

The specific parameters derived within the LVR, including critical strain (γ_c), linear viscoelastic moduli (G'_{LVR}) and (G''_{LVR}), damping factor (tan δ_{LVR}), yield stress (σ_y), and complex viscosity (η^*_{LVR}) are summarized in Table 2. WPIFs Pickering emulsion showed the maximum G'_{LVR} (1468.900 ± 69.721 Pa) and G''_{LVR} (161.065 ± 5.933 Pa) at pH 5.0, indicating significantly enhancement in the viscoelasticity of WPIFs Pickering emulsion at pH 5.0. This phenomenon could be attributed to the aggregation of WPIFs at pH 5.0. γ_c is employed to evaluate the maximum structural strength and deformation resistance of Pickering emulsion. The stress of the γ_c corresponds to the σ_y, which reflects the stress triggers the non-linear deformation (Anvari et al., 2016).η^* and tanδ are important parameters for investigating the emulsion stability against coalescence and creaming (Zhang et al., 2022). As depicted in Table 2, WPIFs Pickering emulsions at pH 5.0 exhibited the highest G'_{LVR} and G''_{LVR} values, corresponding to greater rigidity and higher critical stress. The lower tan δ_{LVR} values and higher η^*_{LVR} values suggested more consistent and elastic structures of WPIFs Pickering emulsion at pH 2.0–3.0.

Dynamic frequency sweep measurements were performed over an angular frequency range of 1–100 rad/s at a constant strain of 0.01% to investigate the viscoelastic properties of the WPIFs Pickering emulsions. Fig. 7(B) depicts G′ and G″ of WPIFs Pickering emulsion at pH 2.0–8.0 as a function of angular frequency (1–100 rad/s). G′ portrays the solid-like elastic characteristics of the Pickering emulsion, and G″ presents the liquid-like viscous characteristics of the Pickering emulsion. As

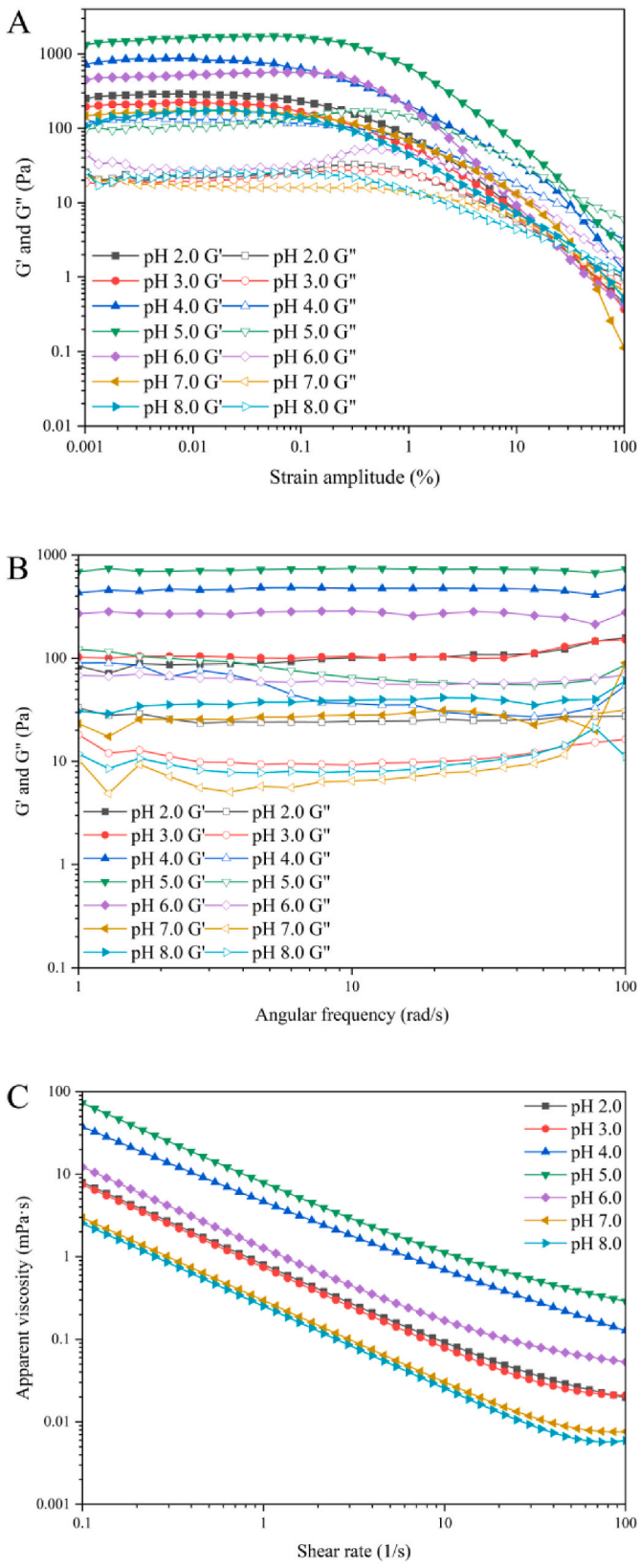

Fig. 7. Strain sweep (A), frequency sweep (B), and flow curve (C) of WPIFs-stabilized Pickering emulsions at pH 2.0–8.0.

presented in Fig. 7(B)–G′ exhibited only a slight dependence on angular frequency, indicating that WPIFs Pickering emulsion exhibited strong elastic properties. With the exception of Pickering emulsion at pH 7.0, G′ consistently exceeded G″ across the entire frequency range, suggesting that the WPIFs Pickering emulsion (excluding pH 7.0) exhibited the solid-like elastic characteristics. Similar findings have been reported by Liu, Liu, et al. (2024). The intersection of G′ and G″ was defined as the gel-to-solid transition point. At pH 7.0, G″ surpassed G′ for WPIFs Pickering emulsion at the high frequency, which was attributed to the rearrangement and flow of emulsion droplets within the system.

Fig. 7(C) depicts the apparent viscosity of WPIFs Pickering emulsion at pH 2.0–8.0 as the function of shear rates (0.1–100 s^{-1}). The apparent viscosity of all WPIFs Pickering emulsions decreased steadily as the shear rate increased, demonstrating the distinct shear thinning behavior, which is consistent with the non-Newtonian pseudoplastic fluids characteristics. This phenomenon can be account for the structural damage and disordered arrangement of emulsion droplets as shear rate increased, leading to a decrease in the apparent viscosity of WPIFs Pickering emulsion at the high shear rates (Jiang, Pan, et al., 2022). In addition, the pH of WPIFs had a significant impact on the apparent viscosity of WPIFs Pickering emulsion. The apparent viscosity of WPIFs Pickering emulsions followed the order: pH 5.0 > pH 4.0 > pH 6.0 > pH 2.0 > pH 3.0 > pH 7.0 > pH 8.0. WPIFs Pickering emulsions were observed to have higher apparent viscosity at pH 5.0 and 4.0 compared with those at pH 7.0 and 8.0. A similar trend was observed in microstructure observations, larger droplet sizes and uneven droplet distribution could increase the number of droplets per unit volume and the interaction between droplets, thereby enhancing the apparent viscosity of the Pickering emulsion. Furthermore, the aggregation of WPIFs at pH 5.0 contributed to the viscosity apparent increased. Aggregated WPIFs accumulate densely on the surface of oil droplets, also resulting in an increase in the viscosity of the Pickering emulsion.

4. Conclusion

In conclusion, pH played a crucial role in determining the structural features of WPIFs, thereby significantly influencing emulsifying properties of WPIFs-stabilized Pickering emulsions. WPIFs were prepared via long-term acidic thermal treatment at pH 2.0, 85 °C, and 10 h. The structural features of WPIFs and emulsifying properties of WPIFs Pickering emulsions were pH-sensitive. These results showed that WPIFs maintained long fibril structures at pH 2.0–3.0, whereas short fibril structures were observed at pH 7.0–8.0. At pH 4.0–6.0, WPIFs underwent aggregation which resulted in increased particle size and decreased zeta potential, with the most distinct aggregates forming at pH 5.0. The structural features of WPIFs determined the emulsifying properties of WPIFs-stabilized Pickering emulsion. WPIFs exhibited relatively low EAI of 14.84 ± 0.37 m^2/g and high ESI of 93.25 ± 1.54 % at pH 5.0. Correspondingly, Pickering emulsion stabilized by aggregated WPIFs had a wider size distribution at pH 5.0, exhibiting high storage modulus, loss modulus, and apparent viscosity. This phenomenon was ascribed to the fact that pH 5.0 is close to the isoelectric point of WPIFs, leading to the formation of a thicker interfacial film at the oil-water interface via the clustering of WPIFs.

CRediT authorship contribution statement

Caiyun Cheng: Writing – original draft, Software, Investigation. **Qian Xu:** Validation. **Yang Li:** Methodology, Investigation. **Eric Haubruge:** Methodology, Investigation. **Ning Liao:** Supervision, Data curation. **Guangsu Zhu:** Supervision, Investigation. **Kunlun Liu:** Writing – review & editing, Supervision, Resources, Methodology, Conceptualization.

Table 2
Viscoelastic parameters of WPIFs-stabilized Pickering emulsions at pH 2.0–8.0.

pH	G'_{LVR} (Pa)	G''_{LVR} (Pa)	Tan (δ) $_{LVR}$	γ_c (%)	σ_y (Pa)	η^*_{LVR} (Pa·S)
2.0	268.210 ± 3.988^{d}	23.318 ± 0.641^{d}	0.087 ± 0.004^{e}	0.037 ± 0.007^{cd}	0.099 ± 0.019^{d}	42.848 ± 0.624^{d}
3.0	212.500 ± 2.814^{de}	20.779 ± 0.561^{de}	0.098 ± 0.004^{de}	0.028 ± 0.005^{d}	0.059 ± 0.011^{d}	33.982 ± 0.437^{de}
4.0	649.030 ± 23.264^{b}	117.170 ± 0.042^{b}	0.181 ± 0.007^{a}	0.088 ± 0.018^{cd}	0.575 ± 0.097^{c}	104.967 ± 3.642^{b}
5.0	1468.900 ± 69.721^{a}	161.065 ± 5.933^{a}	0.110 ± 0.009^{cd}	0.208 ± 0.042^{b}	3.052 ± 0.474^{a}	235.189 ± 10.927^{a}
6.0	414.275 ± 45.177^{c}	51.812 ± 1.578^{c}	0.126 ± 0.018^{c}	0.369 ± 0.075^{a}	1.524 ± 0.148^{b}	66.453 ± 7.103^{c}
7.0	147.530 ± 4.921^{e}	16.051 ± 0.120^{e}	0.109 ± 0.018^{cde}	0.117 ± 0.023^{c}	0.172 ± 0.029^{cd}	23.619 ± 0.777^{e}
8.0	162.365 ± 5.296^{e}	24.872 ± 0.665^{d}	0.153 ± 0.009^{b}	0.049 ± 0.010^{cd}	0.081 ± 0.014^{d}	26.143 ± 0.817^{e}

Note: Different letters represent significant differences ($P < 0.05$).

Declaration of competing interest

We declare that we have no financial and personal relationships with other people or organizations that can inappropriately influence our work, there is no professional or other personal interest of any nature or kind in any product, service and/or company that could be construed as influencing the position presented in, or the review of, the manuscript entitled.

Acknowledgments

This work was supported by the National Natural Science Foundation of China (32172259, 32472381), the Key Research and Development Project of Henan Province (231111111800), and the Program for the Top Young Talents of Henan Associate for Science and Technology (2021).

Data availability

Data will be made available on request.

References

Anvari, M., Tabarsa, M., Cao, R., You, S., Joyner, H. S., Behnam, S., & Rezaei, M. (2016). Compositional characterization and rheological properties of an anionic gum from alyssum homolocarpum seeds. *Food Hydrocolloids, 52*, 766–773. https://doi.org/10.1016/j.foodhyd.2015.07.030

Cao, Y., & Mezzenga, R. (2019). Food protein amyloid fibrils: Origin, structure, formation, characterization, applications and health implications. *Advances in Colloid and Interface Science, 269*, 334–356. https://doi.org/10.1016/j.cis.2019.05.002

Chang, H. W., Tan, T. B., Tan, P. Y., Abas, F., Lai, O. M., Nehdi, I. A., & Tan, C. P. (2017). Formation and characterization of thiol-modified fibrillated whey protein isolate solution with enhanced functionalities. *Journal of Food Engineering, 214*, 277–286. https://doi.org/10.1016/j.jfoodeng.2017.07.015

Chen, D., Fang, F., Federici, E., Campanella, O., & Jones, O. G. (2020). Rheology, microstructure and phase behavior of potato starch-protein fibril mixed gel. *Carbohydrate Polymers, 239*, Article 116247. https://doi.org/10.1016/j.carbpol.2020.116247

Chen, D., Pinho, L. S., Federici, E., Zuo, X., Ilavsky, J., Kuzmenko, I., Yang, Z., Jones, O. G., & Campanella, O. (2022). Heat accelerates degradation of β-lactoglobulin fibrils at neutral pH. *Food Hydrocolloids, 124*, Article 107291. https://doi.org/10.1016/j.foodhyd.2021.107291

Cheng, C., Yuan, C., Cui, B., Li, J., & Liu, G. (2024). β-Cyclodextrin based pickering emulsions for α-tocopherol delivery: Antioxidation stability and bioaccessibility. *Food Chemistry, 438*, Article 138000. https://doi.org/10.1016/j.foodchem.2023.138000

Cheng, C., Yuan, C., Cui, B., Lu, L., Li, J., & Sha, H. (2023). Interfacial behavior of cyclodextrins at the oil-water interface of pickering emulsion. *Food Hydrocolloids, 134*, Article 108104. https://doi.org/10.1016/j.foodhyd.2022.108104

Cui, F., McClements, D. J., Liu, X., Liu, F., & Ngai, T. (2022). Development of pH-responsive emulsions stabilized by whey protein fibrils. *Food Hydrocolloids, 122*, Article 107067. https://doi.org/10.1016/j.foodhyd.2021.107067

Farrokhi, F., Badii, F., Ehsani, M. R., & Hashemi, M. (2019). Functional and thermal properties of nanofibrillated whey protein isolate as functions of denaturation temperature and solution pH. *Colloids and Surfaces A: Physicochemical and Engineering Aspects, 583*, Article 124002. https://doi.org/10.1016/j.colsurfa.2019.124002

Farrokhi, F., Badii, F., Ehsani, M. R., & Hashemi, M. (2020). Effect of pH-dependent fibrillar structure on enzymatic hydrolysis and bioactivity of nanofibrillated whey protein. *LWT-Food Science and Technology, 131*, Article 109709. https://doi.org/10.1016/j.lwt.2020.109709

Gao, Z., Zhao, J., Huang, Y., Yao, X., Zhang, K., Fang, Y., Nishinari, K., Phillips, G. O., & Yang, H. (2017). Edible pickering emulsion stabilized by protein fibrils. Part 1: Effects of pH and fibrils concentration. *LWT-Food Science and Technology, 76*, 1–8. https://doi.org/10.1016/j.lwt.2016.10.038

Jansens, K. J., Rombouts, I., Grootaert, C., Brijs, K., Van Camp, J., Van der Meeren, P., Rousseau, F., Schymkowitz, J., & Delcour, J. A. (2019). Rational design of amyloid-like fibrillary structures for tailoring food protein techno-functionality and their potential health implications. *Comprehensive Reviews in Food Science and Food Safety, 18*(1), 84–105. https://doi.org/10.1111/1541-4337.12404

Ji, F., Xu, J., Ouyang, Y., Mu, D., Li, X., Luo, S., Shen, Y., & Zheng, Z. (2021). Effects of NaCl concentration and temperature on fibrillation, structure, and functional properties of soy protein isolate fibril dispersions. *LWT-Food Science and Technology, 149*, Article 111862. https://doi.org/10.1016/j.lwt.2021.111862

Jiang, F., Chen, C., Wang, X., Huang, W., Jin, W., & Huang, Q. (2022a). Effect of fibril entanglement on pickering emulsions stabilized by whey protein fibrils for nobiletin delivery. *Foods, 11*(11), 1626. https://doi.org/10.3390/foods11111626

Jiang, F., Pan, Y., Peng, D., Huang, W., Shen, W., Jin, W., & Huang, Q. (2022b). Tunable self-assemblies of whey protein isolate fibrils for pickering emulsions structure regulation. *Food Hydrocolloids, 124*, Article 107264. https://doi.org/10.1016/j.foodhyd.2021.107264

Ju, Q., Wu, C., Zhou, H., Qin, D., Hu, X., McClements, D. J., & Luan, G. (2024). Roles of soybean β-conglycinin subunit fractions in fibril formation and the effects of glycinin on them. *Food Hydrocolloids, 152*, Article 109906. https://doi.org/10.1016/j.foodhyd.2024.109906

Khan, A. N., & Khan, R. H. (2022). Protein misfolding and related human diseases: A comprehensive review of toxicity, proteins involved, and current therapeutic strategies. *International Journal of Biological Macromolecules, 223*, 143–160. https://doi.org/10.1016/j.ijbiomac.2022.11.031

Koo, C. K., Chung, C., Ogren, T., Mutilangi, W., & McClements, D. J. (2018a). Extending protein functionality: Microfluidization of heat denatured whey protein fibrils. *Journal of Food Engineering, 223*, 189–196. https://doi.org/10.1016/j.jfoodeng.2017.10.020

Koo, C. K., Chung, C., Picard, R., Ogren, T., Mutilangi, W., & McClements, D. J. (2018b). Modulation of physical properties of microfluidized whey protein fibrils with chitosan. *Food Research International, 113*, 149–155. https://doi.org/10.1016/j.foodres.2018.07.012

Lin, Y., Du, H., Roos, Y., & Miao, S. (2023). Binary complexes of whey protein fibers/isolates and fish gelatins for emulsion stabilization. *Food Hydrocolloids, 143*, Article 108880. https://doi.org/10.1016/j.foodhyd.2023.108880

Lin, Y., Roos, Y. H., & Miao, S. (2025). The effect of whey/soy protein fibril systems on the properties of fish gelatin stabilized emulsion gels. *Food Hydrocolloids, 159*, Article 110655. https://doi.org/10.1016/j.foodhyd.2024.110655

Liu, G., Li, W., Qin, X., & Zhong, Q. (2020). Pickering emulsions stabilized by amphiphilic anisotropic nanofibrils of glycated whey proteins. *Food Hydrocolloids, 101*, Article 105503. https://doi.org/10.1016/j.foodhyd.2019.105503

Liu, H., Liu, C., McClements, D. J., Xu, X., Bai, C., Sun, Q., Xu, F., & Dai, L. (2024a). Reinforcement of heat-set whey protein gels using whey protein nanofibers: Impact of nanofiber morphology and pH values. *Food Hydrocolloids, 153*, Article 109954. https://doi.org/10.1016/j.foodhyd.2024.109954

Liu, C., Wang, Y., Dai, X., Zhang, Y., Yang, Y., Jiang, B., Li, D., & Feng, Z. (2024b). Post-self-assemble of whey protein isolation nanofibrils and its contribution to the stability of pickering emulsion. *Food Hydrocolloids, 151*, Article 109766. https://doi.org/10.1016/j.foodhyd.2024.109766

Meng, Y., Jiang, H., Ji, H., Li, X., Julian, M. D., Sang, S., Jin, Z., Wang, J., & Qiu, C. (2024). Co-encapsulation of curcumin and piperine in whey protein isolate fibrils improves their water dispersibility and antioxidant activity. *Food Bioscience, 58*, Article 103750. https://doi.org/10.1016/j.fbio.2024.103750

Meng, Y., Wei, Z., & Xue, C. (2022). Protein fibrils from different food sources: A review of fibrillation conditions, properties, applications and research trends. *Trends in Food Science & Technology, 121*, 59–75. https://doi.org/10.1016/j.tifs.2022.01.031

Mohammadian, M., & Madadlou, A. (2018). Technological functionality and biological properties of food protein nanofibrils formed by heating at acidic condition. *Trends in Food Science & Technology, 75*, 115–128. https://doi.org/10.1016/j.tifs.2018.03.013

Ouyang, K., Xie, H., Wang, Y., Woo, M. W., Chen, Q., Lai, S., Xiong, H., & Zhao, Q. (2023). Whey protein isolate nanofibrils formed with phosphoric acid: Formation, structural characteristics, and emulsion stability. *Food Hydrocolloids, 135*, Article 108170. https://doi.org/10.1016/j.foodhyd.2022.108170

Ouyang, K., Xie, H., Wu, K., Xiong, H., & Zhao, Q. (2024). Improving fermented milk products using pH-responsive whey protein fibrils: A case study on stirred yogurt. *Food Bioscience, 60*, Article 104507. https://doi.org/10.1016/j.fbio.2024.104507

Pang, S., Shao, P., Sun, Q., Pu, C., & Tang, W. (2020). Relationship between the emulsifying properties and formation time of rice bran protein fibrils. *LWT-Food*

Science and Technology, 122, Article 108985. https://doi.org/10.1016/j.lwt.2019.108985

Qi, X., Li, Y., Zhang, W., Shen, M., Chen, Y., Yu, Q., & Xie, J. (2024). Proteolysis improves the foaming properties of rice protein fibrils: Structure, physicochemical properties changes, and application in angel food cake. *Food Chemistry, 437*, Article 137765. https://doi.org/10.1016/j.foodchem.2023.137765

Wang, Z., Deng, Y., Zhang, Y., Wei, Z., Wan, Z., Li, C., Tang, X., Zhao, Z., Zhou, P., Li, P., Liu, G., & Zhang, M. (2023). Impacts of citric acid concentration and pH value on mechanism and rheological properties of cold-set whey protein fibrils hydrogels. *LWT-Food Science and Technology, 183*, Article 114872.

Xu, Q., Cheng, C., Li, Q., Zhu, G., Wei, Y., & Liu, K. (2025a). Comparison of formation and structural characteristics of amyloid fibrils of peanut protein isolate after hydration treatment at different pH. *Food Hydrocolloids, 159*, Article 110599. https://doi.org/10.1016/j.foodhyd.2024.110599

Xu, Q., Cheng, C., Li, Q., Zhu, G., Wei, Y., & Liu, K. (2025b). Concentration-regulated fibrillation of peanut protein: Formation, structural characteristics, and emulsifying properties. *Food Hydrocolloids, 167*, Article 111421. https://doi.org/10.1016/j.foodhyd.2025.111421

Xu, J., Tang, M., Wang, D., Xie, Q., & Xu, X. (2024). Exploring the self-assembly journey of oat globulin fibrils: From structural evolution to modified functionality. *Food Hydrocolloids, 149*, Article 109587. https://doi.org/10.1016/j.foodhyd.2023.109587

Xu, X., Zhang, Y., Han, M., & Guo, Q. (2024). Whey protein fibrils enhance fat-related texture of emulsion systems: Translating structural changes to textural perception. *Food Hydrocolloids, 146*, Article 109208. https://doi.org/10.1016/j.foodhyd.2023.109208

Zeng, X., Wang, Y., Yang, S., Liu, Y., Li, X., & Liu, D. (2024). The functionalities and applications of whey/whey protein in fermented foods: A review. *Food Science and Biotechnology, 33*(4), 769–790. https://doi.org/10.1007/s10068-023-01460-5

Zhang, Y., Lv, X., Abker, A. M., Oh, D. H., Kassem, J. M., Salama, M., & Fu, X. (2024). Research progress of protein fibrils: A review of formation mechanism, characterization and applications in the food field. *Food Hydrocolloids, 155*, Article 110199. https://doi.org/10.1016/j.foodhyd.2024.110199

Zhang, Y., Wang, Y., Zhang, R., Yu, J., Gao, Y., & Mao, L. (2022). Tuning the rheological and tribological properties to simulate oral processing of novel high internal phase oleogel-in-water emulsions. *Food Hydrocolloids, 131*, Article 107757. https://doi.org/10.1016/j.foodhyd.2022.107757

Zhao, J., Chang, B., Hu, Y., Wang, X., Cao, Z., Zhang, Y., Xu, Z., & Sui, X. (2025). Adsorption mechanism of soy protein amyloid fibrils with different morphological structures at the interface of oil-in-water emulsion. *Food Hydrocolloids, 162*, Article 110899. https://doi.org/10.1016/j.foodhyd.2024.110899

Zhao, H., Xu, X., Yuan, B., Qi, B., & Li, Y. (2024). Fibrillation of soy protein isolate in the presence of metal ions: Structure and gelation behavior. *Food Chemistry, 453*, Article 139672. https://doi.org/10.1016/j.foodchem.2024.139672

Zheng, Y., Gao, Y., Chang, Y., Sun, C., & Fang, Y. (2023). Concentration-regulated fibrillation of soy protein: Structure and in vitro digestion. *Journal of Agricultural and Food Chemistry, 71*(29), 11170–11179. https://doi.org/10.1021/acs.jafc.3c02206

Zheng, F., Yang, Q., Yuan, C., Guo, L., Li, Z., Zhang, J., Nishinari, K., & Cui, B. (2024). Characterizations of corn starch edible films reinforced with whey protein isolate fibrils. *Food Hydrocolloids, 147*, Article 109412. https://doi.org/10.1016/j.foodhyd.2023.109412

Zhu, F. (2024). Modifications of whey proteins for emulsion based applications: Current status, issues and prospectives. *Food Research International, 178*, Article 113935. https://doi.org/10.1016/j.foodres.2024.113935